UC Berkeley
UC Berkeley Previously Published Works

Title

Deep Unsaturated Zone Contributions to Carbon Cycling in Semiarid Environments

Permalink

Journal

ISSN

Authors

Wan, Jiamin
Tokunaga, Tetsu K
Dong, Wenming
et al.

Publication Date

DOI

Peer reviewed

Deep Unsaturated Zone Contributions to Carbon Cycling in Semiarid Environments

Jiamin Wan[1], Tetsu K. Tokunaga[1], Wenming Dong[1], Kenneth H. Williams[1], Yongman Kim[1], Mark E. Conrad[1], Markus Bill[1], William J. Riley[1], and Susan S. Hubbard[1]

[1] Earth and Environment Sciences Area, Lawrence Berkeley National Laboratory, Berkeley, CA, USA

Correspondence to: J. Wan, jwan@lbl.gov

Abstract

Understanding terrestrial carbon cycling has relied primarily on studies of topsoils that are typically characterized to depths shallower than 0.5 m. At a semiarid site instrumented down to 7 m, we measured seasonal- and depth-resolved carbon inventories and fluxes and groundwater and unsaturated zone flow rates. Measurements showed that ~30% of the CO_2 efflux to the atmosphere (60% in winter) originates from below 1 m, contrary to predictions of less than 1% by Earth System Model land modules. Respiration from deeper roots and deeper microbial communities is supported by favorable subsurface temperatures, moisture, and oxygen availability. Below 1 m, dissolved organic carbon fluxes from the overlying soil and C from deep roots and exudates are expected to be important in sustaining microbial respiration. Because these conditions are characteristic of semiarid climate regions, we contend that Earth System Model land modules should incorporate such deeper soil processes to improve CO_2 flux predictions.

1 Introduction

Understanding global carbon cycling and its linkages to climate change requires knowledge of carbon fluxes through different subsurface compartments, including soil, the underlying deep vadose zone, and groundwater, which together constitute the reservoir for most of the climate-change relevant terrestrial carbon stocks (Ahlstrom et al., 2015; Scharlemann et al., 2014; Wang et al., 2010). However, much less is known about carbon fluxes through deeper strata where about half of the Earth's terrestrial carbon inventory resides (Davidson et al., 2011), especially in semiarid and arid regions, which represent about 40% of the Earth's land surface (Ahlstrom et al., 2015). In desert shrublands, the average depth of soil respiration can exceed 0.5 m and be primarily attributable to roots (Breecker et al., 2012). In spite of the importance of soil carbon dynamics to climate change over the next century (Friedlingstein et al., 2014), predictions of soil carbon cycling using Earth System Models (ESMs) remain uncertain (Todd-Brown et al., 2013) with simplified representation of key processes, for example. decomposition (Bonan et al., 2013), transport (Tang et al., 2013; Zhu & Riley, 2015), and nutrient controls (Zaehle et al., 2014; Zhu et al., 2016). Moreover, ESMs are unable to represent spatial

heterogeneities that may affect large-scale carbon exchanges with the atmosphere. Links between quantifying carbon stocks and modeling carbon fluxes through subsoil compartments of terrestrial ecosystems need to be strengthened. Relative to knowledge about near-surface soil (Kaiser & Kalbitz, 2012) and inland aquatic (Battin et al., 2009) carbon processes, less is known about carbon cycling within the subsurface compartments that link those systems, namely, the deep unsaturated zone and groundwater.

The fate of carbon below the surface soil is difficult to investigate because instrumentation, sampling, and understanding flow and transport all become more challenging at greater depths. Although there are a number of studies with deep profile measurements in semiarid regions, a wide range of surface CO_2 fluxes have been reported (Walvoord et al., 2005; Wood et al., 1993). Particularly difficult aspects of subsoil investigations include characterizing mobile inventories of dissolved organic carbon (DOC; Davidson et al., 2011; Mei et al., 2012; Rumpel & Kogel-Knabner, 2011; Sanderman & Amundson, 2008), transformations by deeper microbial communities (Holden & Fierer, 2005), and susceptibility of deeper organic carbon (OC) to mineralization (Kuzyakov, 2010). While OC concentrations are generally lower in semiarid and arid regions, the proportion of total OC (TOC) inventories residing at greater depths is often larger than in more humid regions (Wang et al., 2010). Moreover, deeper profile OC transport and mineralization directly influences bicarbonate levels, often the major anion in semiarid and arid environments. Indeed, semiarid and arid regions commonly contain high levels of carbonate minerals, often to great depths (Monger et al., 2015). However, the low magnitudes and high variability (Walvoord et al., 2005) in recharge through arid and semiarid region profiles make it difficult to study subsurface fluxes of DOC and dissolved inorganic carbon (DIC).

In order to obtain a more comprehensive understanding of C cycling between the soil and deeper subsurface, we conducted an intensive investigation at a site situated along the Colorado River in the semiarid Colorado Plateau. Our related recent work focused primarily on the unique field instrumentation and field-based measurements of CO_2 fluxes (Tokunaga et al., 2016). The present study integrates a larger suite of measurements and analyses including (1) quantification of the subsurface carbon inventory, (2) further analyses of seasonal and depth-dependent CO_2 fluxes, (3) laboratory incubation measurements on seasonal and depth-dependent respiration rates in soils and sediments from multiple locations, and especially (4) the measuring of DOC and DIC fluxes from unsaturated zone pore waters into groundwater. We then compared the results with ESM predictions.

2 Methodology

2.1 Site Description

The study site is situated along the Colorado River in the semiarid Colorado Plateau (Figures 1a and 1b). Drought-tolerant perennial grasses (primarily tall wheatgrass, *Elymus elongatum*, and western wheatgrass, *Pascopyrum*

smithii) and shrubs are the dominant vegetation. Roots are common within the upper meter and sparsely distributed down to 2 m below ground surface (bgs). Excursions in groundwater elevation accompany seasonal variations in Colorado River discharge, with the water table rising from a depth of about 3.5 to 2 m bgs during the transition from baseflow conditions to peak discharge in late spring, respectively; groundwater elevations decline rapidly as discharge wanes, returning to baseflow levels by mid-winter. For simplicity, we divide the subsurface into three stratigraphic compartments: soil (surface to 1.0 m), deep unsaturated zone (1.0 to 3.5 m), and aquifer (3.5 to 7.0 m, always water-saturated), and refer to the entire region above the aquifer (surface to 3.5 m) as the unsaturated zone.
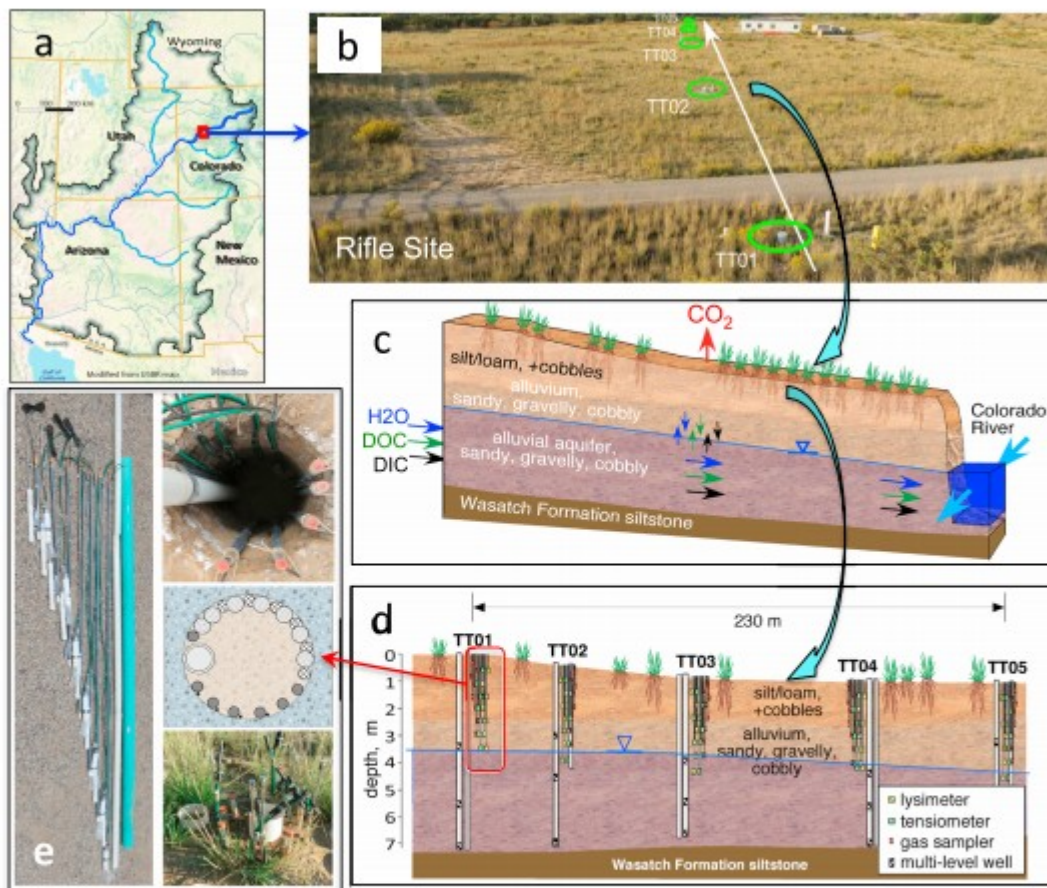

Figure 1. The study site and field instrumentation.(a and b) The semiarid field site near Rifle, Colorado. (c) Compartments and net carbon flux directions. (d and e) Instrumentation transect for measuring carbon inventories and fluxes. Drought-tolerant perennial grasses and shrubs are the dominant vegetation. The water table is typically at a depth of ~3.5 m, and the average groundwater velocity is ~0.3 m d^{-1}. Five monitoring stations were established along a 250-m transect aligned with the groundwater flow direction. Monitoring instruments included thermistors, tensiometers, piezometers, soil water samplers, and gas samplers at multiple depths as well as ground surface flux chambers.

The site's mean annual precipitation is 292 mm (about 50% as snow), and its monthly average potential evaporation ranges from 0 (December through February) up to 135 mm in July (DOE, 1999). The net annual recharge ranges

from 0 to 0.05 m yr^{-1}(Christensen et al., 2018; Tokunaga et al., 2016). The increases in unsaturated zone water storage mainly occur during the months of November to March, when the precipitation exceeds potential evapotranspiration. Additional infiltration occurs in April through June from precipitation and snowmelt. The groundwater flows with reported pore water velocities that range from 0.1 to 0.8 m d^{-1}(Williams et al., 2011). The cobbly loam soil extends to depths of about 1 to 1.5 m bgs, where it transitions to coarse sandy to cobbly alluvium (Shroba & Scott, 1997) interspersed with finer grained and locally organic-rich sediments (Arora et al., 2016; Campbell et al., 2012; Yabusaki et al., 2011). This coarse alluvium extends to the depth of ~7 m and includes the upper aquifer. The depth of the groundwater table is typically ~3.5 m from the soil surface but can rise to as shallow as 2.0 m for about a week in late spring through early summer because of the annual snowmelt-driven rise of the Colorado River.

In order to track water flow, DOC and DIC transport, and gas diffusion through the subsurface, five monitoring/sampling stations were installed with instrumentation at 0.50-m depth intervals, along a 250-m transect aligned with the groundwater flow direction (Figures 1c and 1d). At each of the stations, a 0.254-m diameter borehole was cored to the depth of 3.5 m using waterless sonic drilling (ASTM, 2004; Figure 1e). This method was chosen because it allowed drilling through the coarse sediment that contains large sized cobbles and recovery of sediments in nearly intact cores. With depth-stratification preserved, the excavated material was reused partly for laboratory studies and partly for backfilling around instruments at the same depth interval. Instrument sets at each depth included a tensiometer, matric potential sensor with thermistor, soil water sampler, and gas sampler. The deepest instrumented depth at each site was 3.50 m beneath the soil surface, with progressively shallower sets of instruments installed at 0.50-m vertical separation distances (Tokunaga et al., 2016). Another borehole at each monitoring site was drilled down to the bottom of the upper aquifer (~7-m depth) for groundwater sampling with three levels of samplers. Tensiometer and water table elevation measurements were obtained periodically to track infiltration, evapotranspiration, and seasonal water table fluctuations (Tokunaga et al., 2016). Subsurface temperature profiles were continuously recorded at a series of depths from 0.20 to 6.0 m (Figures 1d and 1e). Pore waters within the unsaturated zone and groundwater were collected for chemical analyses at 2- to 4-week intervals. Soil gas samples from different depths were obtained at approximately monthly intervals. CO$_2$ fluxes at the ground surface were measured periodically during the year through four permanently installed collars at each site. To obtain the daily average rates of CO$_2$ fluxes, long-term chambers (LI-8100A, LI-COR, Lincoln, Nebraska, USA) were used for hourly measurements over the course of several days during spring, summer, and fall.

For use in laboratory studies, soil samples from surface to 1.0-m depth were retrieved using a 0.10-m diameter soil auger with liners. The deeper samples

were collected by waterless sonic drilling described previously (Tokunaga et al., 2016), sampled from interior regions of cored materials to avoid contamination. Cobbles encountered in deeper sediments were excluded. The samples were double bagged and immediately shipped back to the laboratory in sealed plastic buckets with ice. Various analyses of the soil/sediment were conducted including the TOC and TIC concentrations. To further test field measurements of overall CO_2 production and its depth dependence, we conducted a set of laboratory incubation-respiration experiments on soil and deepvadose zone samples (the <4.75-mm grain size fraction) collected from five different depths from four stations. Physical and chemical properties of the samples used are presented in Table S1 in the supporting information. For each of the depths, the soils/sediments were cycled through four temperatures representative of characteristic seasonal values (a simplification based on measurements presented in Figure 3b). More experimental details are presented in the supporting information. The >4.75-mm grain size fraction increased with depth and was excluded from the incubation samples because of its likely very low surface area, OC, and microbial activity. In order to estimate equivalent respiration rates in the field, the laboratory-measured rates were scaled down by factors equal to the depth-dependent mass fraction of <4.75-mm material. The gravel/cobble-corrected bulk densities used to convert mass-based respiration rates to volume-based rates had uncertainties of about 10%.

To calculate subsurface CO_2 fluxes, the diffusion gradient method employing Fick's law at discrete depth intervals was used. The effective diffusion coefficient was calculated with the water-induced linear reduction model developed by Moldrup et al. (2000),

$$D_e = D_o \theta_a^{2.5} F^{-1} \tag{1}$$

where θ_a is the air-filled porosity, F is the total porosity, and D_o is the diffusion coefficient for CO_2 in the bulk air phase. Uncertainties in D_e can become large because of the need to estimate F and θ_a, with the latter approximated as being nonhysteretic with respect to matric potential. However, field and laboratory measurements helped constrain D_e. First, F was determined to decrease with depth based on the increase in the gravel + cobble fraction with depth. Then, θ_a was calculated from field measured matric potential profiles combined with laboratory measured moisture characteristics (water content versus matric potential) scaled to account for the volume fraction occupied by gravel and cobbles. By systematically applying best independent estimates of parameters, the general variation of D_e with changes in field moisture regimes was obtainable. The bulk air phase diffusion coefficient for CO_2 was calculated based on Massman's (1998) relation.

$$D_o = \left(1.381 \times 10^{-5} \text{ m}^2 \text{ s}^{-1}\right) \left(101.325 \text{ kPa/P}\right) \left(T(z,t)/273.15 \text{ K}\right)^{1.81} \tag{2}$$

where P is the average local atmospheric pressure of 83.7 kPa and T (z,t) is the time-dependent temperature at a specific depth z (obtained from thermistors). More details are in the supporting information.

To compare the measurements with the model predictions, we performed the CLM4.5 simulations using the standard CLM protocol (Koven et al., 2013), which includes a multicentury spin up to equilibrium at 1850 using repeated climate forcing (Qian et al., 2006) and then a transient historical simulation with dynamic CO_2 concentrations, nitrogen and aerosol deposition, and land use.

3 Experimental Results and Discussion

The measured depth-dependent C inventories in soil and sediment are presented in Figures 2a and 2b, consisting of low levels of TOC (averaging 2.4 ± 0.2 g C kg^{-1}) and moderate concentrations of TIC (averaging 7.7 ± 1.1 g C kg^{-1} predominantly as $CaCO_3$). The vertical profiles of TOC are relatively uniformly distributed, similar to profiles reported for other semiarid regions (Batjes, 1996; Jobbagy & Jackson, 2000; Wang et al., 2010). These profiles are very different from the more hyperbolic depth distribution of C in humid regions, as shown in Wang et al. (2010), who compared SOC concentrations down to 3.0 m in soils of forests and grasslands versus in shrubland and desert soils. However, no data were previously available on C concentrations and fluxes associated with the mobile pore waters. Over a 2-year period, we sampled pore waters from soils, underlying deeper unsaturated zone, and in groundwater to directly measure DOC and DIC. The DIC concentrations (Figure 2d) were generally higher than DOC and reached maximum concentrations at the water table (~3.5-m depth), reflecting respiration (primarily microbial with some root contribution), CO_2 enrichment and dissolution in the deep unsaturated zone, and dissociation to form bicarbonate. We found relatively high DOC concentrations of 2 to 5 mM throughout the unsaturated zone, 5 to 10 times greater than DOC concentrations in groundwater (~0.4 mM; Figure 2c). It is worth noting that DOC and DIC concentrations from directly sampled field pore waters are seldom reported, and values presented here do not account for carbon in suspended particulates (>1 µm). Besides the measured high DOC concentrations in pore waters, additional desorbable OC from the solid phase (Figure 2a) contributes to the labile OC pool, such that the mobile OC inventory is larger than that indicated by the DOC profiles (Figure 2c). The measured microbial humification index (Dong et al., 2017) profiles of the pore water samples indicate that the deeper DOC is primarily of surface soil and rhizosphere origin, likely transported by snowmelt and rainfall infiltration into the deeper unsaturated zone during late spring to early summer. Note that due to the relatively high salinity of the pore waters, the humification index is the only available speciation method that did not require presample treatment to remove salts. Such pretreatment results in losses of large fractions of DOC, thus impart unknown biases in C speciation. The identification of a high concentration DOC flux from the rhizosphere into the

deep unsaturated zone would not have been possible based on only the conventional bulk soil sampling and analyses (Figure 2a).
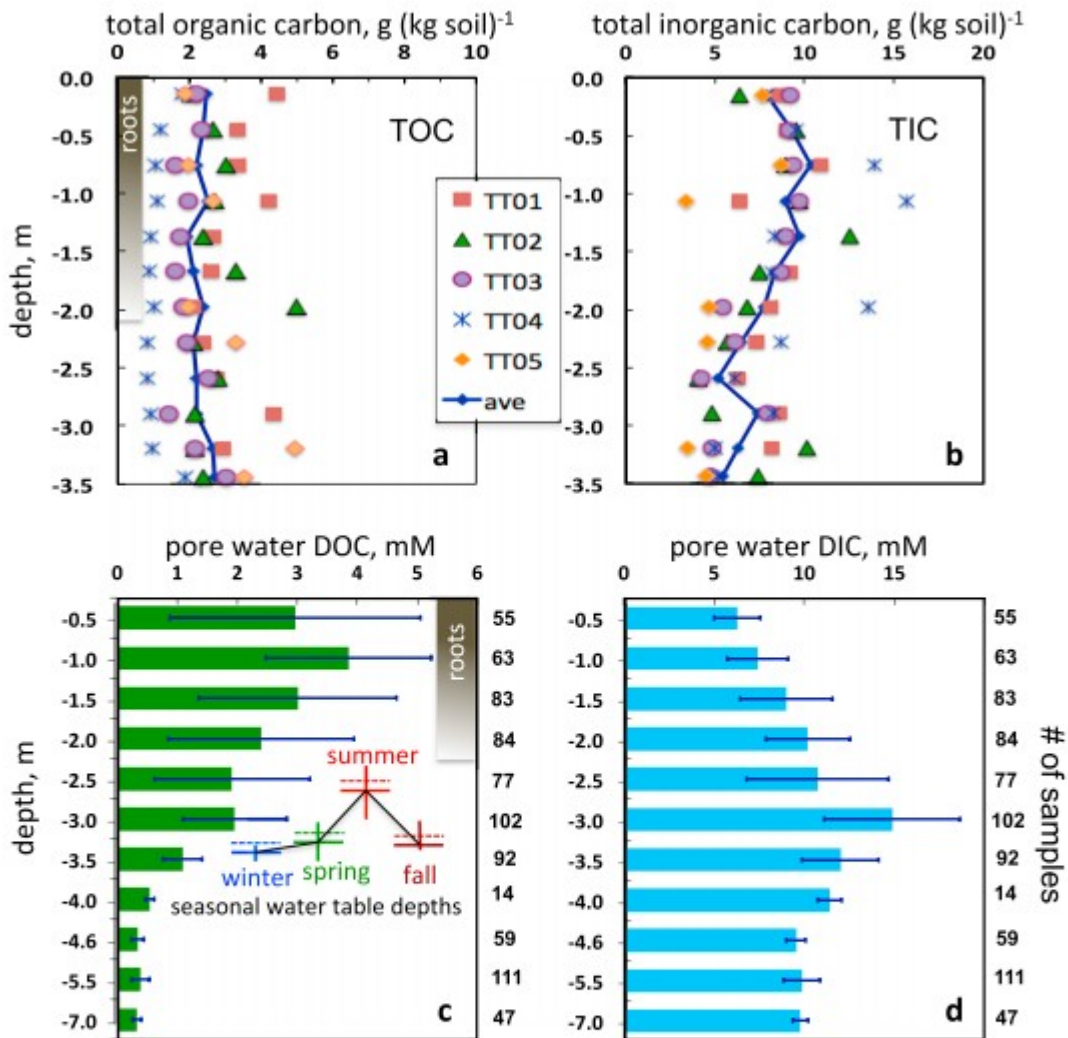

Figure 2. Depth dependence of the subsurface C inventory at the study site, showing unexpected high dissolved organic carbon (DOC) concentrations in the unsaturated zone above the water table. (a and b) Total organic and inorganic C in soil and deep unsaturated zone of <4.7-mm fraction. TT0# refer to the five sampling stations (Figure 1d). (c and d) DOC and dissolved inorganic carbon concentrations in directly collected field pore waters sampled over 2 years. The value at each depth is the average of the samples collected from all stations. The error bars indicate standard deviations. The number of samples collected at each depth is shown along the right y axis. During drier months, the shallower samplers do not yield pore waters. The distribution of observed roots, denser at shallow depths, is indicated by the vertical bars in (a) and (c). In (c), the seasonal variations in average water table and capillary fringe depths are indicated by color-coded horizontal solid and dashed lines, respectively, while the vertical lines indicate ranges of depths within each season.

The measured field temporal and depth-dependent CO_2 fluxes are presented in Figure 3a. The CO_2 fluxes exhibited strong seasonal patterns, with highest fluxes during late spring into summer and lowest fluxes during the winter. The average measured surface CO_2 flux of 330 ± 90 g C m^{-2} yr^{-1} ($n = 620$) is within the midrange of values reported for semiarid regions (184 to 491 g C m^{-2} yr^{-1}; Tokunaga et al., 2016). CO_2 concentration in the deep unsaturated zone seasonally reached as high as 10% of the total gas composition (Figure

3a), partly because of long diffusion distances to the soil surface. The CO_2 concentration maxima typically occurred about 0.5 m above the water table and suggest that active microbial respiration in the deep unsaturated zone is enabled by availability of moisture and OC, favorable moderate temperatures throughout the year (Figure 3b), and sufficient aeration throughout most of the year (Figure 3c). Organic C supplied by groundwater into the deeper vadose zone during annual water table rise is not expected to contribute significantly to respired C because of the relatively low DOC concentrations in groundwater (Figure 2c). On the other hand, annual water table decline is expected to stimulate both microbial and root respiration through drawing in O_2 from the vadose zone. The pore gas O_2 concentrations generally decreased with increased CO_2 and with depth but always remained greater than 3 mole %, sufficient to maintain aerobic respiration (Greenwood, 1961). Measured depth profiles of subsurface CO_2 concentrations and estimated diffusion coefficients were combined in the gradient method (Maier & Schack-Kirchner, 2014) to calculate diffusive fluxes of CO_2 at various depths (section 2). Using this approach, the diffusive flux of CO_2 at the soil surface averaged over the year is 317 g C m^{-2} yr^{-1} (similar to the directly measured surface fluxes of 330 g C m^{-2} yr^{-1}). Further application of the diffusion gradient analysis indicates that a large portion (30% annually) of the CO_2 emissions at the soil surface originated from below 1.0 and above the water table over the course of the year, and that the low winter time respiration has an even higher relative contribution (60%) from this deeper zone (Figure 3d). Roots are sparsely distributed within the 1- to 2-m depth interval and contribute directly to CO_2 production in the deeper zone through root respiration (Breecker et al., 2012), as well as indirectly through microbial degradation of exudates and dead tissue.
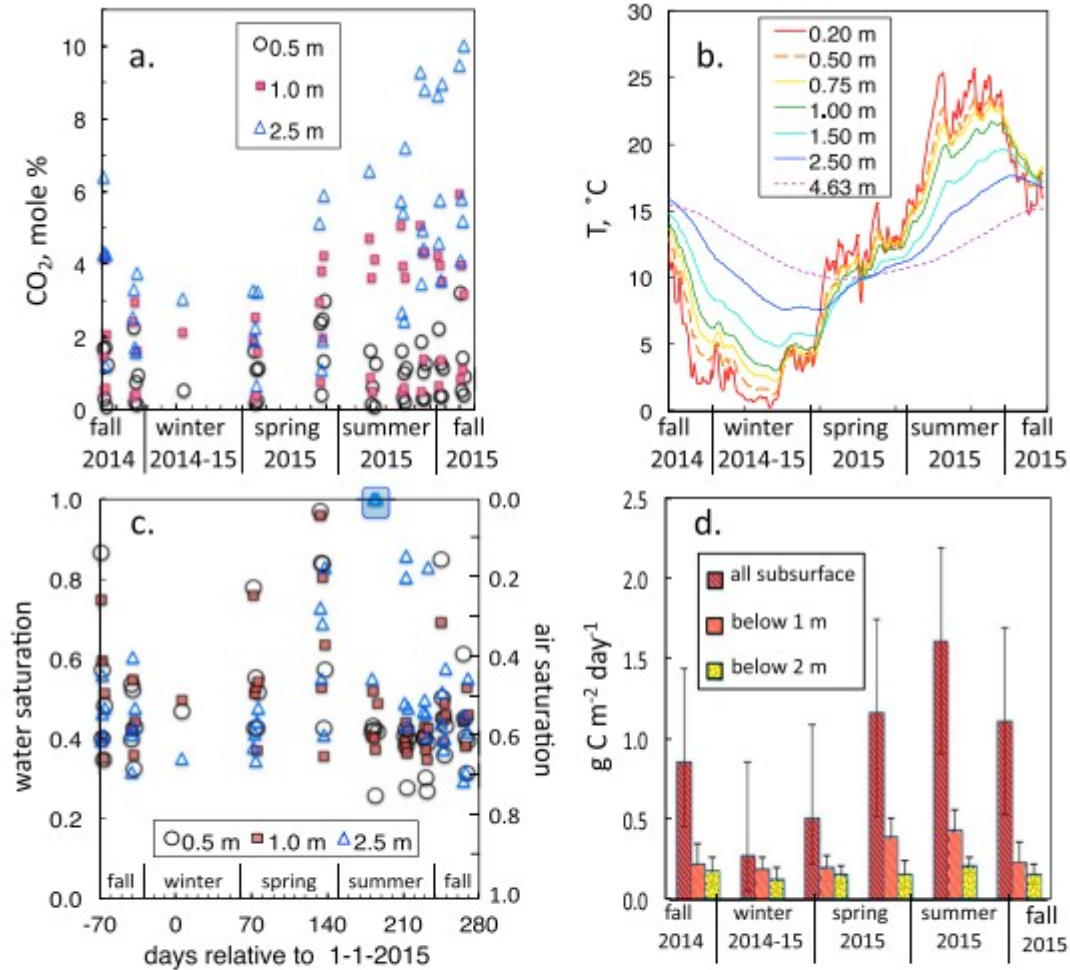
Figure 3. Temporal and depth trends of subsurface CO_2 fluxes, showing significant contributions from below 1 m. (a) CO_2 concentrations (5% relative uncertainties). (b) Temperatures. (c) Volumetric water and air saturations in the soil and deeper subsurface pores (≤10% *relative* uncertainties). Data points in (a) and (c) represent individual values from each of the five stations. Data points within the blue box (c) denote water saturation = 1 for most of the 2.50-m depths during brief inundation from water table rise. (d) Diffusion-calculated CO_2 fluxes (averages from five stations). CO_2 fluxes originating from below 1 m contribute 30% of the total annual flux and are relatively more important during winter (up to 60%).

These field-based results suggesting that favorable environmental conditions (DOC, temperature, moisture, and O_2) in the deeper unsaturated zone support relatively high CO_2 production rates motivated the laboratory incubation measurements (section 2 and more details in the supporting information). The depth- and season-dependent average steady state CO_2 production rates measured in the laboratory incubation experiment are summarized in Figure 4a. All sterilized samples showed zero CO_2 production. The ^{13}C analyses of the headspace gases from the incubation jars (unsterilized soil sample) show distinctly biogenic isotopic signatures (Figure S1 in the supporting information). Together, these data demonstrate that CO_2 efflux is predominantly attributable to respiration throughout the entire unsaturated zone, and CO_2 production rates of the deep unsaturated zone (1.0 to 3.6 m, above the water table) are relatively high. A profile-integrated

respiration rate of 270 g C m^{-2} yr^{-1} was obtained, in fair agreement with the field-measured surface effluxes of carbon (326 g C m^{-2} yr^{-1}) and the diffusion-estimated surface effluxes (317 g C m^{-2} yr^{-1}). Laboratory respiration rates are expected to be lower than field-based measurements because of the exclusion of root respiration. The daily CO_2 fluxes integrated for all depths and for fluxes originating in depth ranges of 0–1 m, 1–2 m, 2–2.6 m, and 2.6–3.6 m show strong seasonal variation and decline with depth (Figure 4b). Although the higher respiration rate in the surface soil is expected, these results also indicate that depths between 1 and 2 m, and 2 and 3.5 m annually account for about 30% and 15%, respectively, of the surface CO_2 effluxes (Figure 4c). Note that in wintertime 60% of the emitted CO_2 originated from below 1 m. The incubation inferred depth and temporal CO_2 production trends (Figure 4b) are consistent with those from the field-inferred values (Figure 3d). Q10 values from the laboratory incubations (Table S2) averaged over the four seasons decreased from 4.1 at the surface (0–0.15 m) down to 1.2 in the deep unsaturated zone (2.6–3.6 m).
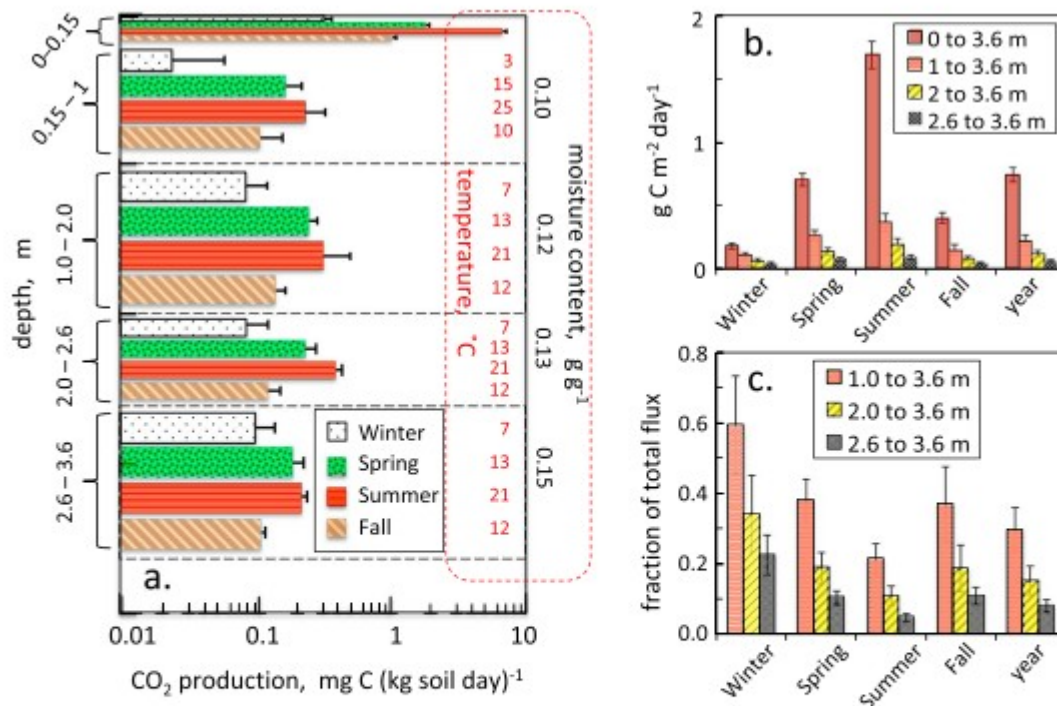

Figure 4. Depth- and season-dependent respiration rates from incubated samples (four samples per depth), showing large contributions from below 1 m, consistent with field measurements.(a) Depth profile of CO_2 production rates (averages of samples from four stations). The numbers along the right axis are seasonal incubation temperatures (for simplicity only one set of temperatures was used for 0–1.0 m and another set for 1.0–3.6 m). Incubation moisture contents (based averages from field samples) are also shown on the right axis.(b) CO_2 production rates, comparing full profiles (0–3.6 m) with rates evolved below 1-, 2-, and 2.6-m depths.(c) Fraction of total CO_2 production originating below selected depths. Control samples were sterilized by gamma radiation and produced no CO_2. The properties of the sediment samples are presented in Table S1.

4 Extrapolations

These field- and laboratory-based results provide the basis for evaluating overall carbon fluxes in the subsurface of this semiarid environment, with a focus on depths below 1 m, and to compare these measurement-based fluxes with ESM predictions. Exports of carbon were determined based on field measured and calculated diffusive CO_2 fluxes (Figure 3d), laboratory determined respiration rates (Figure 4), DIC and DOC concentrations from the directly sampled pore waters (Figures 2c and 2d), and the estimated infiltration rates and groundwater velocities. These measurements were applied to a volume aligned with the transect (Figure 5), having a longitudinal extent of 250 m, a depth of 7 m, and unit width (1.0 m). It should be noted that measurements of net primary production needed to complete the carbon mass balance were beyond the scope of this study. Nevertheless, the importance of vadose zone exports to the atmosphere and groundwater become evident through analyses of fluxes at the transect scale.
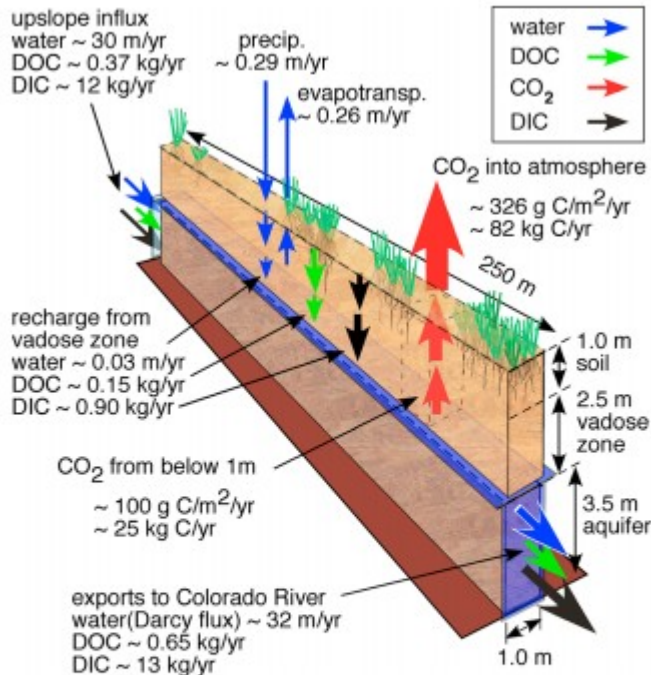

Figure 5. Estimated carbon fluxes and balance along the measurement transect, showing 30% of annual CO_2 emissions from deeper than 1.0 m, contrary to predictions of <1% by the Earth System Models. The dissolved organic carbon flux from the rhizosphere throughout the unsaturated zone as well as favorable subsurface environmental conditions are responsible for supporting respiration in the deep unsaturated zone.

The total respiration flux leaving the 250-m^2 reference soil surface was 82 kg C yr^{-1}, equivalent to 328 g C m^{-2} yr^{-1}. The diffusion gradient analysis and the gradient method indicate a large fraction, annually ~30% of the total CO_2 efflux, originated from below 1 m and above the water table. Opposing this net upward carbon flux in the gas phase are low magnitude downward fluxes

of DIC and DOC. While infiltration through the surface soil largely occurs in late spring through early summer, high overall evapotranspiration reduces the net deep recharge to only about 0.03 m yr^{-1} (unsaturated pore water velocity ~0.15 m yr^{-1}). This net recharge rate multiplied by unsaturated zone pore water concentrations yield rates of DIC and DOC transport into groundwater of about 0.9 and 0.15 kg yr^{-1}, respectively. Although carbon transported to the river consisted of high DIC (bicarbonate) concentrations of ~10 mM, and moderate DOC concentrations of ~0.4 mM, these exports were limited by the groundwater flow velocity. Combining an effective aquifer porosity of 0.27 with a groundwater velocity estimated to average about 0.30 m per day (Williams et al., 2011) yields a Darcy velocity of 32 m yr^{-1}. With this groundwater flux, annual exports of DIC and DOC into the river per m of shoreline amounted to about 13 and 0.65 kg, respectively.

We compared these estimates with predictions from the ESM land model CLM4.5 (Ghimire et al., 2016; Koven et al., 2013; Figure S2). Globally, CLM4.5 predicts that less than 1% of the surface CO_2 flux originates below 1-m depth. Also, CLM4.5 does not explicitly represent advective DOC or DIC fluxes (nor to our knowledge does any land model integrated in an ESM), which we argue here are main mechanisms responsible for sustained C availability at depth.

Notwithstanding the very low CO_2 fluxes originating from below 1 m predicted by ESMs, several factors support our findings of higher respiration rates in the deeper subsurface. As noted previously, this deeper zone is characterized by favorable temperature, moisture, and O_2 levels throughout the year and receives pulses of OC from the shallower soil zone during major recharge events. The presence of deeper roots, albeit sparsely distributed (Jackson et al., 1996), further contributes to CO_2 production, indirectly through supply of OC and directly through respiration. Given the common occurrence of all of the above factors, we contend that ESM land models need to incorporate these deeper soil processes to improve CO_2 flux predictions in semiarid climate regions.

Acknowledgments

References

Ahlstrom, A., Raupach, M. R., Schurgers, G., Smith, B., Arneth, A., Jung, M., et al. (2015). The dominant role of semi-arid ecosystems in the trend and variability of the land CO_2 sink. *Science*, 348(6237), 895– 899. https://doi.org/10.1126/science.aaa1668

Arora, B., Spycher, N. F., Steefel, C. I., Molins, S., Bill, M., Conrad, M. E., et al. (2016). Influence of hydrological, biogeochemical and temperature transients on subsurface carbon fluxes in a flood plain environment. *Biogeochemistry*, 127(2–3), 367– 396. https://doi.org/10.1007/s10533-016-0186-8

ASTM (2004). Standard practices for sonic drilling for site characterization and installation of subsurface monitoring devices, ASTM, D 6914-04, 1–11.

Batjes, N. H. (1996). Total carbon and nitrogen in the soils of the world. *European Journal of Soil Science*, 47(2), 151– 163. https://doi.org/10.1111/j.1365-2389.1996.tb01386.x

Battin, T. J., Kaplan, L. A., Findlay, S., Hopkinson, C. S., Marti, E., Packman, A. I., et al. (2009). Biophysical controls on organic carbon fluxes in fluvial networks (vol 1, pg 95, 2008). *Nature Geoscience*, 2(8), 595– 595. https://doi.org/10.1038/ngeo602

Bonan, G. B., Hartman, M. D., Parton, W. J., & Wieder, W. R. (2013). Evaluating litter decomposition in Earth System Models with long-term litterbag experiments: an example using the Community Land Model version 4 (CLM4). *Global Change Biology*, 19(3), 957– 974. https://doi.org/10.1111/Gcb.12031

Breecker, D. O., McFadden, L. D., Sharp, Z. D., Martinez, M., & Litvak, M. E. (2012). Deep autotrophic soil respiration in shrubland and woodland ecosystems in Central New Mexico. *Ecosystems*, 15(1), 83– 96. https://doi.org/10.1007/s10021-011-9495-x

Campbell, K. M., Kukkadapu, R. K., Qafoku, N. P., Peacock, A. D., Lesher, E., Williams, K. H., et al. (2012). Geochemical, mineralogical and microbiological characteristics of sediment from a naturally reduced zone in a uranium-contaminated aquifer. *Applied Geochemistry*, 27(8), 1499– 1511. https://doi.org/10.1016/j.apgeochem.2012.04.013

Christensen, J. N., Dafflon, B., Shiel, A. E., Tokunaga, T. K., Wan, J., Faybishenko, B., et al. (2018). Using strontium isotopes to evaluate the spatial variation of groundwater recharge. *Science of the Total Environment*, 637, 672– 685.

Davidson, E., Lefebvre, P. A., Brando, P. M., Ray, D. M., Trumbore, S. E., Solorzano, L. A., et al. (2011). Carbon inputs and water uptake in deep soils of an Eastern Amazon forest. *Forest Science*, 57(1), 51– 58.

DOE (1999). Final site observational work plan for the UMTRA Project Old RIfle Site*Rep. GJO-99-88-TAR Rev. 1* (122 pp.) Grand Junction, CO, U.S. Dept. of Energy.

Dong, W., Wan, J., Tokunaga, T. K., Gilbert, B., & Williams, K. H. (2017). Transport and humification of dissolved organic matter within a semi-arid floodplain. *Journal of Environmental Sciences*, (57), 24– 32. https://doi.org/10.1016/j.jes.2016.12.011

Friedlingstein, P., Meinshausen, M., Arora, V. K., Jones, C. D., Anav, A., Liddicoat, S. K., & Knutti, R. (2014). Uncertainties in CMIP5 climate projections due to carbon cycle feedbacks. *Journal of Climate*, 27(2), 511– 526. https://doi.org/10.1175/JCLI-D-12-00579.1

Ghimire, B., Riley, W. J., Koven, C. D., Mu, M., & Randerson, J. T. (2016). Representing leaf and root physiological traits in CLM improves global carbon and nitrogen cycling predictions. *Journal of Advances in Modeling Earth Systems*, 8(2), 598– 613. https://doi.org/10.1002/2015MS000538

Greenwood, D. J. (1961). The effect of oxygen concentration on the decomposition of organic materials in soil. *Plant and Soil*, 14(4), 360– 376. https://doi.org/10.1007/BF01666294

Holden, P. A., & Fierer, N. (2005). Microbial processes in the vadose zone. *Vadose Zone Journal*, 4(1), 1– 21. https://doi.org/10.2136/vzj2005.0001

Jackson, R. B., Canadell, J., Ehleringer, J. R., Mooney, H. A., Sala, O. E., & Schulze, E. D. (1996). A global analysis of root distributions for terrestrial biomes. *Oecologia*, 108(3), 389– 411. https://doi.org/10.1007/BF00333714

Jobbagy, E. G., & Jackson, R. B. (2000). The vertical distribution of soil organic carbon and its relation to climate and vegetation. *Ecological Applications*, 10(2), 423– 436. https://doi.org/10.2307/2641104

Kaiser, K., & Kalbitz, K. (2012). Cycling downwards—Dissolved organic matter in soils. *Soil Biology and Biochemistry*, 52, 29– 32. https://doi.org/10.1016/j.soilbio.2012.04.002

Koven, C. D., Riley, W. J., Subin, Z. M., Tang, J. Y., Torn, M. S., Collins, W. D., et al. (2013). The effect of vertically resolved soil biogeochemistry and alternate soil C and N models on C dynamics of CLM4. *Biogeosciences*, 10(11), 7109– 7131. https://doi.org/10.5194/Bg-10-7109-2013

Kuzyakov, Y. (2010). Priming effects: Interactions between living and dead organic matter. *Soil Biology & Biochemistry*, 42(9), 1363– 1371. https://doi.org/10.1016/j.soilbio.2010.04.003

Maier, M., & Schack-Kirchner, H. (2014). Using the gradient method to determine soil gas flux: A review. *Agricultural and Forest Meteorology*, 192, 78– 95. https://doi.org/10.1016/J.Agrformet.2014.03.006

Massman, W. J. (1998). A review of the molecular diffusivities of H2O, CO2, CH4, CO, O-3, SO2, NH3, N2O, NO, AND NO2 in air, O-2 AND N-2 near STP. *Atmospheric Environment*, 32(6), 1111– 1127. https://doi.org/10.1016/S1352-2310(97)00391-9

Mei, Y., Hornberger, G. M., Kaplan, L. A., Newbold, J. D., & Aufdenkampe, A. K. (2012). Estimation of dissolved organic carbon contribution from hillslope soils to a headwater stream. *Water Resources Research*, 48, W09514. https://doi.org/10.1029/2011WR010815

Moldrup, P., Olesen, T., Gamst, J., Schjonning, P., Yamaguchi, T., & Rolston, D. E. (2000). Predicting the gas diffusion coefficient in repacked soil: Water-induced linear reduction model. *Soil Science Society of America Journal*, 64(5), 1588– 1594. https://doi.org/10.2136/sssaj2000.6451588x

Monger, H. C., Kraimer, R. A., Khresat, S., Cole, D. R., Wang, X. J., & Wang, J. P. (2015). Sequestration of inorganic carbon in soil and groundwater. *Geology*, 43(5), 375– 378. https://doi.org/10.1130/G36449.1

Qian, T. T., Dai, A., Trenberth, K. E., & Oleson, K. W. (2006). Simulation of global land surface conditions from 1948 to 2004. Part I: Forcing data and evaluations. *Journal of Hydrometeorology*, 7(5), 953– 975. https://doi.org/10.1175/Jhm540.1

Rumpel, C., & Kogel-Knabner, I. (2011). Deep soil organic matter-a key but poorly understood component of terrestrial C cycle. *Plant and Soil*, 338(1–2), 143– 158. https://doi.org/10.1007/s11104-010-0391-5

Sanderman, J., & Amundson, R. (2008). A comparative study of dissolved organic carbon transport and stabilization in California forest and grassland soils. *Biogeochemistry*, 89(3), 309– 327. https://doi.org/10.1007/s10533-008-9221-8

Scharlemann, J. P. W., Tanner, E. V. J., Hiederer, R., & Kapos, V. (2014). Global soil carbon: Understanding and managing the largest terrestrial carbon pool. *Carbon Management*, 5(1), 81– 91. https://doi.org/10.4155/cmt.13.77

Shroba, R. R., &Scott, R. B. (1997), Revised preliminary geologic map of the Rifle quadrangle, Garfield County, Colorado*Rep. Open File Report 97–852*, *1–20 pp*, *Denver*, *Colorado*, *U.S. Geological Survey*.

Tang, J. Y., Riley, W. J., Koven, C. D., & Subin, Z. M. (2013). CLM4-BeTR, a generic biogeochemical transport and reaction module for CLM4: model development, evaluation, and application. *Geoscientific Model Development*, 6(1), 127– 140. https://doi.org/10.5194/Gmd-6-127-2013

Todd-Brown, K. E. O., Randerson, J. T., Post, W. M., Hoffman, F. M., Tarnocai, C., Schuur, E. A. G., & Allison, S. D. (2013). Causes of variation in soil carbon simulations from CMIP5 Earth System Models and comparison with observations. *Biogeosciences*, 10(3), 1717– 1736. https://doi.org/10.5194/bg-10-1717-2013

Tokunaga, T. K., Kim, Y., Conrad, M. E., Bill, M., Hobson, C., Williams, K. H., et al. (2016). Deep Vadose zone respiration contributions to carbon dioxide fluxes from a semiarid floodplain. *Vadose Zone Journal*, 15(7). https://doi.org/10.2136/vzj2016.02.0014

Walvoord, M. A., Striegl, R. G., Prudic, D. E., & Stonestrom, D. A. (2005). CO2 dynamics in the Amargosa Desert: Fluxes and isotopic speciation in a deep unsaturated zone. *Water Resources Research*, 41, W02006. https://doi.org/10.1029/2004WR003599

Wang, Y., Li, Y., Ye, X., Chu, Y., & Wang, X. (2010). Profile storage of organic/inorganic carbon in soil: From forest to desert. *Science of the Total Environment*, 408(8), 1925– 1931. https://doi.org/10.1016/j.scitotenv.2010.01.015

Williams, K. H., Long, P. E., Davis, J. A., Wilkins, M. J., N'Guessan, A. L., Steefel, C. I., et al. (2011). Acetate availability and its influence on sustainable bioremediation of uranium-contaminated groundwater. *Geomicrobiology Journal*, 28(5–6), 519– 539. https://doi.org/10.1080/01490451.2010.520074

Wood, B. D., Keller, C. K., & Johnstone, D. L. (1993). In situ measurement of microbial activity and controls on microbial CO_2 production in the unsaturated zone. *Water Resources Research*, 29, 647– 659. https://doi.org/10.1029/92WR02315

Yabusaki, S. B., Fang, Y. L., Williams, K. H., Murray, C. J., Ward, A. L., Dayvault, R. D., et al. (2011). Variably saturated flow and multicomponent biogeochemical reactive transport modeling of a uranium bioremediation field experiment. *Journal of Contaminant Hydrology*, 126(3–4), 271– 290. https://doi.org/10.1016/j.jconhyd.2011.09.002

Zaehle, S., Medlyn, B. E., de Kauwe, M. G., Walker, A. P., Dietze, M. C., Hickler, T., et al. (2014). Evaluation of 11 terrestrial carbon-nitrogen cycle models against observations from two temperate free-air CO2 enrichment studies. *The New Phytologist*, 202(3), 803– 822. https://doi.org/10.1111/nph.12697

Zhu, Q., Iversen, C. M., Riley, W. J., Slette, I. J., & Vander Stel, H. M. (2016). Root traits explain observed tundra vegetation nitrogen uptake patterns: Implications for trait-based land models. *Journal of Geophysical Research: Biogeosciences*, 121, 3101– 3112. https://doi.org/10.1002/2016jg003554

Zhu, Q., & Riley, W. J. (2015). Improved modeling of soil nitrogen losses. *Nature Climate Change*, 5(8), 705– 706. https://doi.org/10.1038/nclimate2696